Decentralized Power Management of Multiple PV, Battery, and Droop Units in an Islanded Microgrid

Hisham Mahmood, *Member, IEEE,* and Jin Jiang, *Fellow, IEEE*

Abstract—In this paper, a decentralized power management strategy is proposed for multiple PV, battery, and droop units in an islanded microgrid. The control strategy is developed to handle any combination of these units without modifying their control systems. This provides a more comprehensive and generalized approach to coordinate the three types of units, in comparison to the techniques in the literature that consider only two types, mainly PV and battery systems, or consider only a single unit of each type. The operation of each unit is autonomously coordinated to maintain the balance between generation and consumption, while ensuring controlled charging/discharging of the batteries in the microgrid. To achieve this coordination, the voltage and the power control loops, within each of the PV and battery units, are configured to follow the specifically designed multi-segment power/frequency (*P/f*) characteristic curves. These characteristics are designed to independently adapt to the microgrid operating conditions, without relying on any external communications and centralized management systems. Accordingly, the control system for each unit is able to autonomously and seamlessly switch in real-time between power control and frequency regulation based on the available PV power, the *SOC* of the batteries, and the total load demand in the microgrid The strategy is designed and implemented using multi-loop controllers, in contrast to the commonly adopted approach of using discrete operating modes and switching logics. The proposed strategy is validated using a microgrid simulated in PSCAD/EMTDC with detailed switching models of the power electronic converters.

Index Terms—Microgrid, power management, droop control, PV, battery storage.

I. INTRODUCTION

THE intermittent nature of photovoltaic (PV) power generation poses a great challenge to the widespread adoption of PV systems in islanded microgrids. This necessitates the deployment of battery systems to complement the intermittent generation of PV units in order to maintain power balance in islanded microgrids. In other words, battery systems mimic the role the utility grid plays in grid-connected microgrids, to supply/absorb needed/surplus energy. However, battery systems have limited power ratings, limited capacities, and restricted charging scenarios that depend on the battery state-of-charge (*SOC*). Therefore, the operation of the PV and battery units must be coordinated to consider both the intermittent PV generation and the operating constraints of the battery units. Moreover, PV and battery units must be able to coordinate with

H. Mahmood is with the College of Engineering, Mathematics, and Physical Sciences, University of Exeter, Cornwall, TR10 9EZ, UK. (e-mail: h.mahmood@exeter.ac.uk)

J. Jiang are with the Department of Electrical and Computer Engineering, The University of Western Ontario, London, ON N6A 5B9, Canada (jjiang@eng.uwo.ca).

dispatchable units that are commonly deployed to ensure continuity of supply. In islanded microgrids, these units typically employ the droop control strategies to achieve appropriate power sharing among the units [1]–[6].

Traditionally, this coordination problem is carried out using centralized control strategies, which commonly require a central energy management system (EMS), and communication links among units [7]–[14]. To be able to coordinate the operation of the microgrid units, the EMS requires access to measurements from each unit and send control commands through communications. Therefore, a communication failure in even a single unit may disrupt the operation of the entire microgrid, as this unit can no longer be accessed or influenced by the EMS. Accordingly, relying on communication channels for power management can be a key factor affecting the system reliability [2], [3].

The other approach to this coordination task is through decentralized, or so-called autonomous, power management. In this approach, local controllers on different units are co-operatively responsible for the microgrid power management, without direct information exchange with other units and/or an EMS. Decentralized power management of PV and battery units has attained prominent attention in recent years [15]–[23]. A simple microgrid with only a single battery unit and a PV unit is considered in [15], whereas multiple PV units and a battery unit are considered in [16]. The control strategies developed in [15], [16] are limited to microgrids with only one battery unit dedicated to regulate the microgrid frequency. This also makes the strategies inapplicable to microgrids containing conventional droop controlled units.

The ability of PV and battery units to coordinate with conventional droop controlled units is not considered in any of the control strategies presented in [15]–[17], [22]. However, dispatchable droop controlled units are widely employed in the literature to ensure supply continuity in the microgrid, and also to exploit the decentralized feature of the droop control concept. Accordingly, to achieve high deployment of PV and battery units in microgrids, their control strategies must be able to work with the widely adopted droop controlled units. An elegant control strategy is proposed in [18] for PV and droop controlled units. However, the power management of battery units is not considered; which makes it inapplicable to PV/battery based microgrids. A control strategy that employs adaptive *P/f* characteristics is proposed in [19], to ensure fully decentralized power management of PV and battery units in a droop controlled microgrid. However, the strategy is specifically designed to coordinate a single PV unit and a single battery unit with multiple droop units.

Power management strategies for PV/battery hybrid units are proposed in [20]–[26]. In a hybrid unit, the PV and battery systems are integrated and deployed as a single system in the microgrid. In this configuration, the control strategy has the advantage of accessing both the PV power measurements and the battery SOC. Therefore, the strategies in [20]–[26] cannot be utilized for decentralized power management of separate PV and battery units in islanded microgrids. In the latter case, each of the PV and battery units must be able to independently coordinate their operation with other units, while cooperatively maintaining the power balance and providing controlled battery charging/discharging. Moreover, the strategy presented in [24] requires a central EMS, under specific conditions, to coordinate the hybrid unit operation with a diesel generator. The control strategies proposed in [25], [26] are specifically designed for a single unit microgrid which, from a control point of view, acts as a standalone power supply. Therefore, they cannot be deployed in multiple-unit microgrids. As in [17], the control strategy proposed in [22] employs discrete control modes and switching logic, which results in a variable structure control system. This structure induces a significant transient and chattering when switching among some control modes. This strategy is focused on the output power flow of the unit, with less attention paid to the control interaction of the unit power converters, and the curtailment controller. For example, to exit the curtailment mode, a logical condition is used to compare the available maximum PV power with the supplied load. However, in practice, the available PV power is unknown during curtailment. Managing the power flow inside the PV unit is a critical task, and its control design must go hand-in-hand with the design of the output stage control system. As will be shown in this paper, two levels of controllers, Primary and Secondary, are used in PV units to manage the power flow, with smooth transients when switching among control objectives.

Note that, each of the above techniques can only accommodate two of the common unit types that are considered in this paper. In most of the existing work, dispatchable droop units have not been considered, although these units are the most common type in islanded microgrids to ensure the continuity of the supply. Deploying only PV and battery units in an islanded microgrid is not realistic in practice. On the other hand, as discussed previously battery units are commonly deployed together with PV units. Moreover, for a coordination strategy to be practical, it should be able to handle multiple units of different types, in a decentralized fashion, with minimum transients when switching among different control objectives/modes.

To overcome the limited applicability and transients drawbacks of the above mentioned techniques, a more comprehensive power management strategy is introduced in this paper to achieve a fully decentralized power management of any combination of PV, battery and droop controlled units. The decentralized coordination is achieved through the proposed multi-loop voltage and power controllers that are implemented locally at each unit. These controllers are configured to follow the proposed multi-segment P/f characteristics, which adapt to the microgrid operating conditions. Accordingly, the control
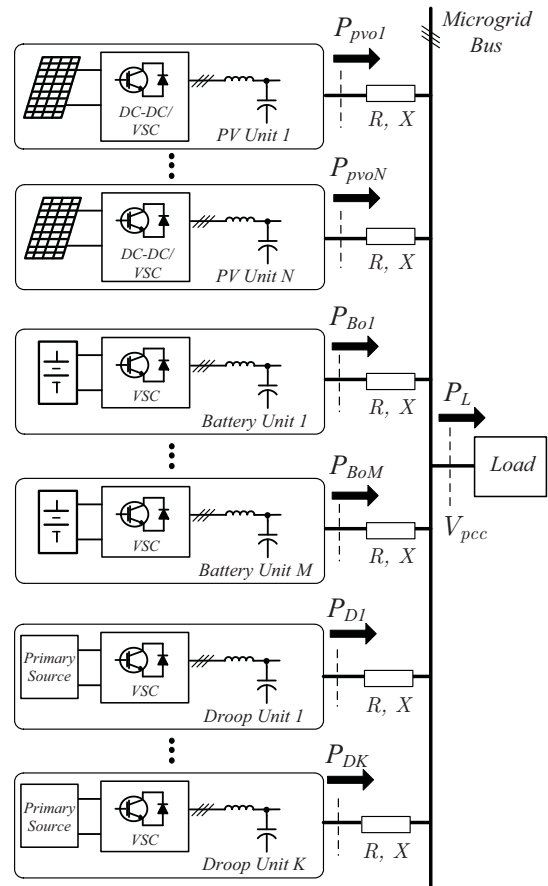

Fig. 1. Composition of the considered islanded microgrid.

system at each unit can independently and seamlessly transfer between power and frequency regulation to maintain the power balance in the microgrid, while ensuring controlled charging/discharging of the batteries. Moreover, the proposed strategy is compatible with the one described in [23], as both of them use the concept of multi-segment P/f characteristics. There, it allows decentralized coordination of PV, battery, and PV/battery hybrid units under a more generalized power management strategy.

The proposed P/f characteristics, the multi-loop control system architecture, and possible microgrid operating scenarios are discussed in Section II. The simulation results of the proposed strategy are presented in Section III, followed by the concluding remarks.

II. PROPOSED CONTROL STRATEGY

The microgrid considered in this paper can be composed of any possible combination of PV units, battery units, and conventional droop controlled units. A general structure is shown in Fig. 1 for a three-phase microgrid with N PV units, M battery units, and K droop units. Each of these units is connected to the microgrid bus using a three-phase voltage sourced converter (VSC). More details on the system structure of each type of these units will be presented later in this section.
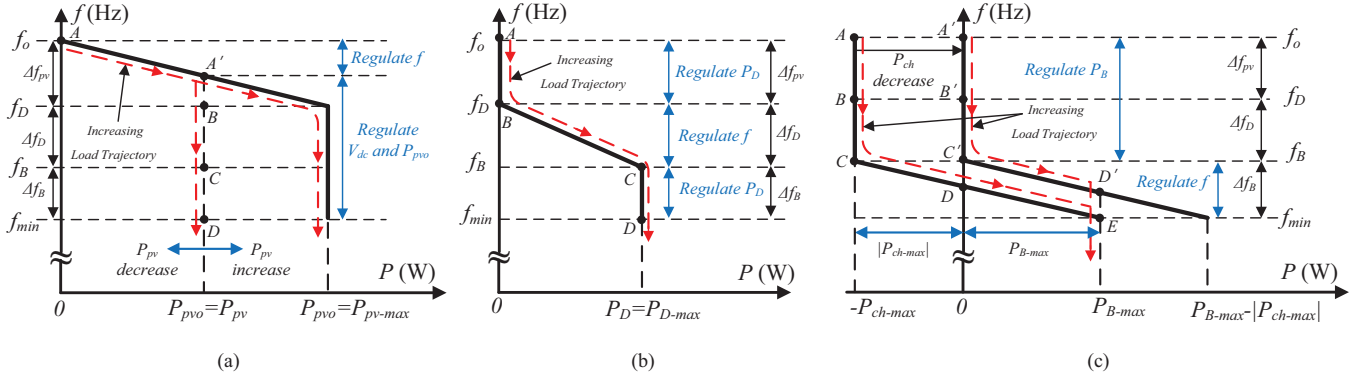
Fig. 2. P/f characteristics of the PV, the battery, and the equivalent single droop unit. (a) PV unit. (b) Droop unit. (c) Battery unit

The proposed multi-loop controllers configure the output P/f characteristics into the multi-segment curves shown in Fig. 2. The microgrid operating frequency range $[f_o, f_{min}]$ is divided into three segments, *PV Segment* (Δf_{pv}), *Droop Segment* (Δf_D), and *Battery Segment* (Δf_B), as indicated in Fig. 2. These segments relate, respectively, to the units that are responsible for regulating the microgrid frequency at any time, i.e. PV, droop controlled, or battery units.

All the droop controlled units are aggregated and then represented in Fig. 2b by a single equivalent unit with the maximum power rating being $P_{D-max} = P_{D1-max} + \cdots + P_{DK-max}$ [19], [21]. Accordingly, the frequency droop coefficient for this unit (m_D) can be represented as

$$m_D = \frac{\Delta f_D}{P_{D1-max} + \cdots + P_{DK-max}} = \frac{\Delta f_D}{P_{D-max}} \qquad (1)$$

A. Control Objectives

The *P/f* characteristics are structured to assign each type of units the following control objectives:

1) PV Units: The main objective of the PV units is to supply all the available PV power, in order to meet the load demand and the charging power required by the battery units. However, these PV units must also maintain the power balance in the islanded microgrid, by considering the load demand at any time, and the different charging characteristics and the *SOC* at each of the battery units without having direct communication with them. Accordingly, the PV units must be able to curtail any surplus power production, and at the same time autonomously follow load variations, and also follow the charging characteristics for each battery unit to maintain the power balance in the whole microgrid, without any direct communication or central power management.

2) Droop Units: The droop units share the load demand and the charging power, only after the PV units reach their maximum available power. This objective is to ensure a full utilization of all available PV power before drawing power from the dispatchable units.

3) Battery Units: The main control objective of the battery units is to coordinate with other units in the microgrid in order to charge the batteries according to their different charging characteristics and SOC levels. The units attempt to achieve this task autonomously whenever there is surplus generation

left after the whole load demand in the microgrid has been met. On the other hand, battery units supply power to the microgrid, only when needed, i.e. after all PV and droop units reach their generation limits. This objective is set to save the stored energy to meet the load demand at nights and during low PV production periods.

To achieve the above challenging objective autonomously, the multi-segment adaptive *P/f* characteristics have been proposed. These characteristics are implemented locally in each unit and can adapt to various operating conditions while seamlessly transitioning between voltage regulation and power control objectives, autonomously without any supervisory control to initiate these transitions.

Since the main focus of this paper is on real power management as in [7]–[10], [12], [15], [20]–[24], [27], conventional reactive power/voltage (Q/V) droop controllers are adopted herein for reactive power management. More comprehensive reactive power control strategies can be found in [28].

B. Basic Operation and Control Actions

The transition of the *P/f* operating points along the *P/f* characteristic curves is determined by the total load in the microgrid, the available PV power, and the total charging power required by the battery units. A detailed illustrative diagram for these three types of units is shown in Fig. 3. The *P/f* characteristic curves, along with the local controller actions in each segment are discussed in the following subsections.

1) PV Segment: The microgrid operates in this segment when the total PV power available in the microgrid is higher than the total load demand, including the charging power for the battery units. The *P/f* characteristic curve of a single PV unit is shown in Fig. 2a for two operating conditions: $P_{pv} < P_{pv-max}$, and $P_{pv} = P_{pv-max}$, where P_{pv} is the PV power available at a given time, and P_{pv-max} is the PV array power rating.

Within this segment, PV units are responsible for regulating the microgrid frequency while sharing the total microgrid load using droop control. In other words, the VSC at each unit regulates the frequency using the *PV Droop Controller* shown in Fig. 3, where the frequency droop coefficient is defined as $m_{pv} = \Delta f_{pv}/P_{pv-max}$. The PV unit continues to meet any increase in the load until it exhausts all the available PV
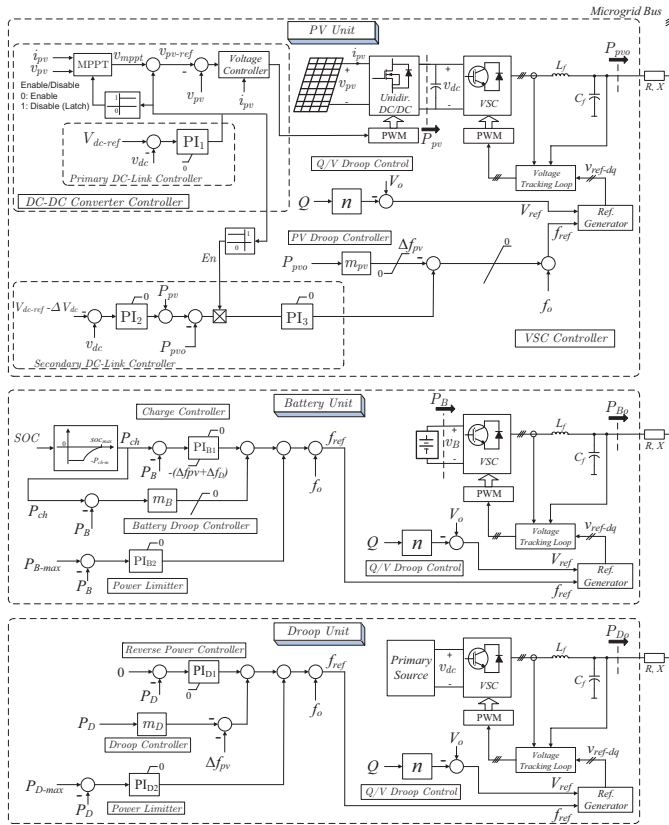
Fig. 3. Detailed control systems for three different types of units.

power to support the load, as illustrated in Fig. 2a by the *P/f* trajectory segment AA'. While operating along this segment, the *Primary DC-Link Controller* shown in Fig. 3, is in charge of regulating the DC-link voltage, by curtailing the surplus PV power. The controller PI_1 curtails the PV power by increasing the PV array terminal voltage away from the maximum power point (MPP). At the same time, the output of the controller PI_1 is used to generate two signals. The first one is used to disable the maximum power point tracking (MPPT) algorithm, by holding its output reference v_{mppt} constant, to prevent it from drifting away from the MPP region. The second signal is used to disable the *Secondary DC-link Controller* since this controller is designed to operate only on the available PV power, not during the curtailment process, as will be discussed in detail in this subsection.

The PI_1 control loop keeps regulating the DC-link voltage by adjusting the PV array operating point in response to any changes in the load or PV power production. This controller reduces the PV voltage to compensate for any increase in the load and/or decrease in the PV power until it reaches its limit at zero, and hence the MPPT algorithm is enabled. At the same time, the *P/f* trajectory reaches point A' where the unit supplies all the available PV power to the microgrid. At this point, the *Secondary DC-Link Controller* is also enabled.

Any further increase in the load will cause the DC-link voltage to drop until it reaches the new reference $V_{dc\text{-}ref} - \Delta V_{dc}$. At this stage, the *Secondary DC-Link Controller* takes charge of regulating the DC-link voltage by regulating the

power delivered to the microgrid (P_{pvo}), through controlling the VSC frequency. Note that, from a control point of view, the measured PV power production P_{pv} employed at the output of the controller PI_2 can be seen as a feed-forward control input to the *Secondary DC-Link Controller*. Also, from a different perspective, the PI_3 control loop can be considered as the main loop with a control error input of ($P_{pv} - P_{pvo}$), while the PI_2 loop is used to compensate for the power losses by maintaining the DC-link voltage regulated at $V_{dc\text{-}ref} - \Delta V_{dc}$.

Meanwhile, the other PV units continue to supply the increased load until they reach their limits. When all PV units reach their production limits, they regulate their output power, by reducing the frequency, until the microgrid enters the *Droop Segment* at point B in Fig. 2a. In summary, the *P/f* characteristic curve of the PV unit is divided into two segments. In the first segment (AA'), the VSC is responsible for regulating the frequency, while the DC-DC converter is in charge of regulating the DC-link. In the second segment ($A'D$), the VSC is in charge of regulating the output power and the DC-link voltage, while the DC-DC converter injects all available power into the DC-link. When the available PV power increases/decreases, the *P/f* segment $A'D$ moves to the right/left accordingly, as indicated in Fig. 2a.

In the PV segment, droop units are controlled to neither supply to nor import power from the microgrid. This control action is represented by the segment AB in Fig. 2b. This is achieved through shifting the frequency droop characteristic curve down by Δf_{pv}, and using the *Reverse Power Controller*, shown in Fig. 3, to prevent reverse power flow into the unit. Note that, this control system is similar to the conventional droop system [29], except that the droop operating range is limited between f_D and f_B instead of f_o and f_{min}, respectively. The *Reverse Power Controller* continues to oppose any reverse power flow until point B, where it reaches its limit at zero. The microgrid starts operating in the *Droop Segment* in response to any further increase in the load.

On the other hand, the battery units operate as power controlled sources in this segment, to import the power required to charge the batteries. This is achieved using the *Charge Controller* shown in Fig. 3. The charging power reference P_{ch} is generated as a function of the battery SOC [19], [30]–[33]. The shape of the charging power curve used in this paper is shown in Fig. 4 [19], [32]. The control action in this segment is presented in Fig. 2c for two cases: $P_{ch} = -P_{ch\text{-}max}$ and $P_{ch} = 0$, using the *P/f* trajectory segments AB and $A'B'$, respectively. Therefore, the battery *P/f* characteristic curve shifts from left to right in Fig. 2c as the charging power P_{ch} decreases from $P_{ch\text{-}max}$ to 0, and the SOC increases from ($SOC_{ref} - \delta SOC$) to SOC_{ref}. As the load increases, the battery units follow the decreasing microgrid frequency to keep importing the required power until the *P/f* trajectory enters the *Droop Segment* as illustrated in Fig. 2c.

2) Droop Segment: In this segment, PV units and battery units continue operating as power controlled sources to regulate their output power at their P_{pv} and P_{ch} references, respectively. On the other hand, the droop units start sharing any increase in the load while regulating the frequency according to their frequency droop curves. In other words, the droop units

become responsible for regulating the microgrid frequency, in this segment. Note that, the *Reverse Power Controllers* in the droop units reach their limit at zero at point B, and hence these controllers cease contributing to the frequency references (f_{ref}) in these units. The droop units reach their power rating limits at the frequency f_B, as indicated by the *P/f* operating point C in Fig. 2b.

3) Battery Segment: The PV units continue regulating their output power at their limits depending on the available PV production at each unit. Similarly, droop units start regulating their output power at their power rating limits using the *Power Limiter* control loop shown in Fig. 3. In other words, both the PV and battery units have reached their limits and can no longer supply any increase in the load demand. On the other hand, the battery units are no longer able to regulate their output power in this segment due to the chosen saturation limits of the *Charge Controller* PI_{B1}. Therefore, the battery units start picking up the increased load in this segment, while regulating the microgrid frequency using the *Battery Droop Controller*. The frequency droop coefficient m_B is set as

$$m_B = \frac{\Delta f_B}{P_{ch\text{-}max} + P_{B\text{-}max}} \tag{2}$$

where $P_{ch\text{-}max}$, and $P_{B\text{-}max}$ are the maximum charging power, and the power rating of the considered battery unit, respectively. The operation of the battery units in this segment is illustrated in Fig. 2c using two cases with different charging power references (under different *SOC* levels). In the first case, represented by the P/f trajectory CDE, the battery is being charged at $P_{ch\text{-}max}$. At point C, any increase in the load demand results in a reduction in the charging power to meet the load, while following the trajectory segment CD. Note that, the reduction in the charging power will be shared among battery units based on their respective droop slopes. At point D, the battery is neither charging nor discharging. For any further increase in the load, the battery unit starts discharging to support the load, following the segment DE. At this point, the unit reaches its output power limit, and therefore starts limiting its output power using the *Power Limiter* loop shown in Fig. 3.

In the second case, a unit with a fully charged battery is considered. This unit will follow the *P/f* trajectory $C'D'E$, shown in Fig. 2c. In this case, the battery starts discharging to supply the increased load, once it enters this segment at point C'. In summary, fully charged units, and units with higher *SOC* start discharging first before other units, which gives higher priority to charging batteries with lower *SOC*. If all the battery units reach their limits, the microgrid frequency will be reduced below f_{min}, through the action of the *Power Limiter* control loops. At this point, a load shedding procedure must be activated [1], which is beyond the scope of this paper.

C. Response Changes in PV Power Production

The operating scenarios discussed so far have considered only the response to changes in the load demand, to explain the basic operation of the control loops. The response of the developed strategy to changes in the PV power production is discussed next.
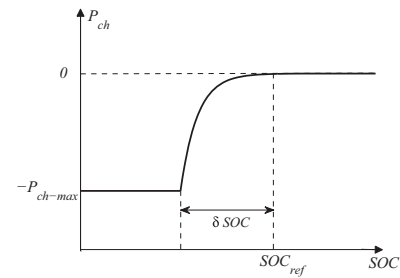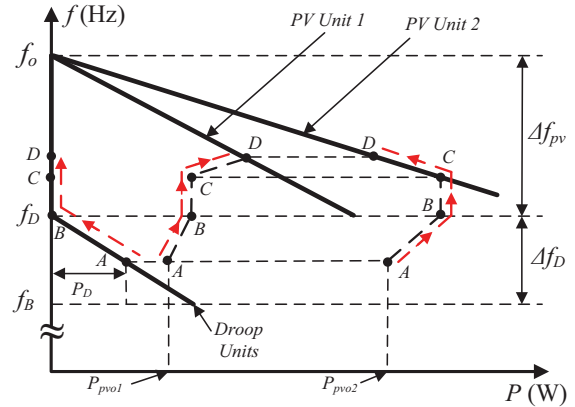

Fig. 4. Battery charging curve.

Fig. 5. Case study scenario illustrating the *P/f* trajectories in response to PV production variations

During the curtailment process, the *Primary DC-Link Controller* in the PV unit keeps adjusting the PV array voltage to regulate the DC-link voltage at $V_{dc\text{-}ref}$. More specifically, when the PV power increases, the DC-link voltage tends to increase and accordingly the controller PI_1 increases the PV array voltage further away from the MPP. At the same time, the segment AD' is shifted further to the right in Fig. 2a. On the other hand, when PV power decreases, the controller PI_1 lowers the PV array voltage to move closer to the MPP, in order to match the supplied load. This continues with any decrease in the PV power until the output of the controller PI_1 reaches zero, and the MPPT algorithm is activated. For any further decrease in the PV power, the DC-link voltage starts dropping until the *Secondary DC-Link Controller* takes control of regulating it at $V_{dc\text{-}ref} - \Delta V_{dc}$, as explained previously.

To illustrate the basic control actions in response to PV power variations, an operating scenario is shown in Fig. 5. The scenario starts with *PV Unit 1* and *PV Unit 2* operating in the *Droop Segment*, while regulating their output powers at P_{pvo1} and P_{pvo2}, respectively. At the same time, the droop units are regulating the microgrid frequency and supplying the rest of the load (P_D). As the PV power increases, the *Secondary DC-Link Controller* in each unit starts to increase the output power, in order to maintain the DC-link voltage regulated at $V_{dc\text{-}ref} - \Delta V_{dc}$. The droop units sense the reduction in their supplied power, and hence increase the frequency according to their frequency droop characteristics. This control action is illustrated by the *P/f* trajectories AB in Fig. 5. At points B, the PV units supply all the microgrid load demand. For

any further increase in the PV power, the *Secondary DC-Link Controller* in both PV units attempts to increase the output power by raising the frequency as illustrated by the trajectories BC. At points C, the output of the controller PI_3 in *PV Unit 2* saturates at zero and the output frequency reference is solely determined by the *PV Droop Controller* in this unit. This can be explained visually by the *P/f* operating point being on the droop line of *PV Unit 2*.

If the PV power increases further, *PV Unit 2* starts operating as a droop unit while the *Primary DC-Link Controller* regulates the DC-link voltage by curtailing the PV power. On the other hand, the *Secondary DC-Link Controller* in *PV Unit 1* increases the supplied power share in response to the increased PV production. Since *PV Unit 2* is operating as a droop unit, it senses a reduction in its supplied load share, and hence increases the frequency accordingly. This process continues until the *P/f* trajectories reach points D. Any further increase in the PV production will be curtailed using the *Secondary DC-Link Controllers*, with no change in the *P/f* operating point, as it is determined by the load at this point. The behavior of the system in response to other possible scenarios can be explained similarly using the *P/f* characteristics, and the multi-loop controllers in Fig. 3.

D. Response to SOC Variations

To further explain the way that multiple battery units interact in response to *SOC* and load variations, two case studies are considered herein. They focus on the autonomous reaction of a battery unit to the *SOC* variations of the same unit, and also to the *SOC* variations at other battery units.

1) Case Study 1: Two battery units are considered in this case: *Battery Unit 1* and *Battery Unit 2*. Initially, the system operates with charging references of $P_{ch1} = -P_{ch1-max}$ and $P_{ch2} = -P_{ch2-max}$, and $SOC_2 > SOC_1$. The *SOC* at each unit is lower than the threshold $SOC_{ref} - \delta SOC$ (see Fig. 4). Initially, both units are charging their batteries at reduced rates with respect to their charging references, as shown in Fig. 6a at points A. This grants a higher priority to supplying the load by the droop units, which supply a portion of the charging power and the load power.

The batteries are being charged at the same rate until SOC_2 becomes equal to $SOC_{ref} - \delta SOC$. Beyond this point, the charging reference P_{ch-2} at *Battery Unit 2* starts decreasing according to the charging curve in Fig. 4. This is equivalent to shifting the *P/f* characteristics of *Battery Unit 2* to the right as the charging power reference decreases from $-P_{ch2-max}$ to $-|P_{ch}|$, as indicated in Fig. 6a. This process results in reducing the charging power share of *Battery Unit 2*, while increasing that of *Battery Unit 1*, which autonomously favors the unit with a lower *SOC*. This action is represented by the *P/f* trajectories AB. Note that, batteries in both units are being charged at reduced rates until points B, where both units start following their charging references, i.e. $P_{B2} = P_{ch2}$ and $P_{B1} = P_{ch1} = -P_{ch1-max}$, as illustrated in Fig. 6a. At points B both units enter the *Droop Segment* and start operating as power controlled sources. Therefore, both battery units start following their charging references along the trajectories BC.

Description	Parameter	Value
Nominal Frequency	f_o	60 Hz
Minimum Frequency	f_{min}	59.7 Hz
PV Segment	Δf_{pv}	0.1 Hz
Droop Segment	Δf_D	0.1 Hz
Battery Segment	Δf_B	0.1 Hz
Battery Capacity	C_{bat}	10 Ah
Battery Converter Rating	P_{B-max}	1000 W
PV Units:		
Unit 1 Power Rating	$P_{pv1-max}$	1000 W
Unit 2 Power Rating	$P_{pv2-max}$	2000 W
Controller PI_1	K_p, K_i	60, 40 (1/s)
Controller PI_2	K_p, K_i	20W/V, 40W/(V·s)
Controller PI_3	K_p, K_i	0.001Hz/W, 0.005Hz/(W·s)
Battery Units:		
Unit 1 Power Ratings	$P_{B1-max}, P_{ch1-max}$	2000 W
Unit 2 Power Ratings	$P_{B2-max}, P_{ch2-max}$	1000 W
Controller PI_{B1}	K_p, K_i	0.001Hz/W, 0.005Hz/(W·s)
Controller PI_{B2}	K_p, K_i	0.0005Hz/W, 0.005Hz/(W·s)
Droop Units:		
Unit 1 Power Rating	P_{D1-max}	1000 W
Unit 2 Power Rating	P_{D2-max}	2000 W
Controller PI_{D1}	K_p, K_i	0.001Hz/W, 0.005Hz/(W·s)
Controller PI_{D2}	K_p, K_i	0.0005Hz/W, 0.005Hz/(W·s)

Note that, at points C, the charging power is negligible according to the charging curve in Fig. 4. The system stays at points C until SOC_1 reaches the threshold $SOC_{ref} - \delta SOC$, and therefore the charging reference for this unit starts decreasing until SOC_1 reaches SOC_{ref} at point D.

2) Case Study 2: This case illustrates the response of the battery units to load changes while operating in the *Battery Segment*. The difference in this scenario is that a step down in the load happens when the system is at points A' in Fig. 6b. Since, both units operate as droop units in this segment, the charging power increases at both units while following the trajectories along droop segments $A'B'$. At points B', both units starts operating as power controlled sources, while following the change in frequency. This frequency change results from the reduction in the load delivered by the droop units due to the load decrease. The rest of the scenario along the trajectories BCD is similar to the situation explained in *Case Study 1*.

III. VALIDATION

A microgrid of six DG units has been simulated in the PSCAD/EMTDC environment, using detailed switching models of the power converters. The microgrid main parameters are listed in Table I.

A. Basic Operation

The performance of the microgrid in response to load variations is validated using the scenario shown in Fig. 7. The considered battery capacities are 20Ah and 10Ah for *Battery Unit 1* and 2, respectively, while the charging profile parameters are set to $SOC_{ref} = 90\%$, and $\delta SOC = 20\%$. The initial *SOC* values are set at 60% and 80% for *Battery Unit 1* and 2, respectively. Therefore, according to the charging profile, the battery in *Unit 2* is being charged at
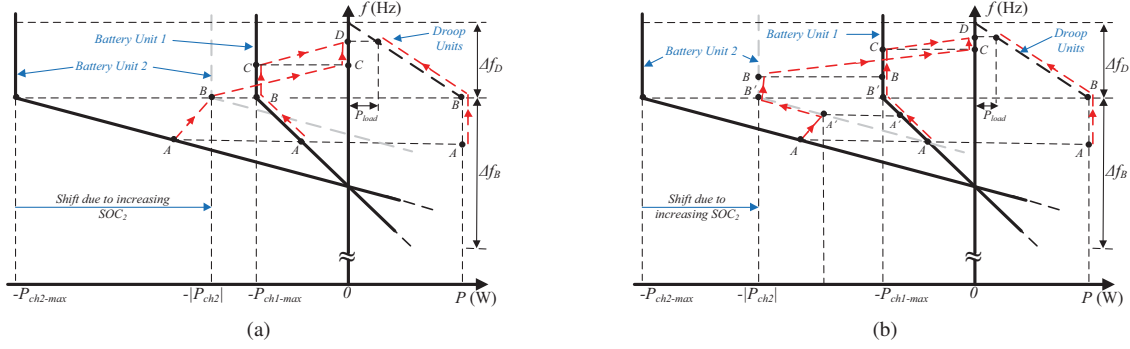
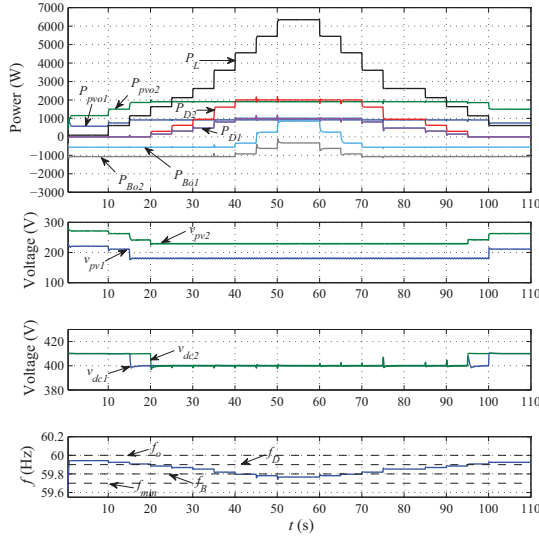Fig. 6. *P/f* trajectory in response *SOC* variations (a) Case Study 1; (b) Case Study 2.

Fig. 7. Coordination of the microgrid units in response to variations in the load demand.

$P_{ch2\text{-}max}$ =1,000W, while the battery in *Unit 1* is being charged at power level of approximately 500W. Initially, at no load, the PV units operate in the *PV Segment*, while providing all the charging power according to their PV droop characteristics in this segment. In both PV units, the surplus PV generation is curtailed using the *Primary DC-Link Controllers*, which regulate the DC-link voltages, v_{dc1} and v_{dc2}, at $V_{dc\text{-}ref} = 410V$. The PV units continue to supply any increase in the load demand, while adjusting their PV array voltages using the *Primary DC-Link Controllers*. At $t = 15s$, *PV Unit 1* reaches its maximum available generation at $v_{pv1} = V_{MPP1} = 230V$. Extra supplied power causes the DC-link voltage at this unit to drop until it reaches $V_{dc\text{-}ref} - \Delta V_{dc} = 400V$. At this point, the *Secondary DC-Link Controller* starts regulating the DC-link voltage, while limiting the output power at this unit. Similarly, *PV Unit 2* reaches its maximum power at $t = 20$ and $v_{pv2} = V_{MPP2} = 180V$.

At this point, the microgrid starts operating in the *Droop Segment*, as can be seen from the microgrid frequency ($f_B < f < f_D$) in Fig. 7. The droop controlled units start sharing the load demand according to their droop characteristics until they reach their maximum rating powers at $t = 40s$. At

this point, the *Power Limiter* control loops start regulating the output power of these units.

The microgrid enters the *Battery Segment* at this point. Therefore, any further increase in the load demand results in reducing the charging power at each unit. Because *Battery Unit 2* has a higher *SOC* of 80%, its *P/f* characteristic curve is shifted more to the right, as illustrated previously in Fig. 2c, and Section II-B3. Accordingly, *Battery Unit 2* starts discharging at $t = 45s$ to meet the load demand, while *Battery Unit 1* continues charging its battery but at a reduced power level. Similarly, the coordination of the DG units in response to a decreasing load demand is shown in Fig. 7 for the period between $t = 60s$ and $t = 100s$.

B. Battery Charging Performance

To validate the performance of the battery charging control systems, an accelerated scenario has been simulated and presented in Fig. 8. In this scenario the charging parameter δSOC is reduced to 1%, and the battery capacities are reduced to half of their original capacities, in order to illustrate the charging performance in a relatively short simulation time. Initially, the *SOC* values are 88.4% and 88.3% for *Battery Unit 1* and 2, respectively. In this scenario, the microgrid operates in the *Battery Segment*, with both battery units are being charged at reduced power levels in order to meet the load demand in the microgrid. At $t = 22s$, the *SOC* in *Unit 1* exceeds $SOC_{ref} - \delta SOC = 89\%$, which results in a decreased charging power at *Battery Unit 1*, and an increased charging power at *Battery Unit 2*, as illustrated previously using the *P/f* trajectory of AB in Fig. 6a, or AA' in Fig. 6b. At $t = 40s$, a step down in the load occurs, which causes both units to reach their charging power references, as illustrated using the *P/f* trajectory $A'B'$ in Fig. 6b. Also, the output power delivered by the droop units decreases to follow the load demand. At this point, the microgrid operates in the *Droop Segment*, where the battery units operate as power controlled units to follow their own charging references. As the total charging power reduces with time in response to the increasing *SOC* levels, the power delivered by the droop units reduces accordingly. Also, as can be seen in Fig. 8, the battery units keep following their charging references regardless of the load changes at $t = 60s$ and 80s. At $t = 80s$, the PV units start curtailing their generation to follow the decreasing load, as the battery
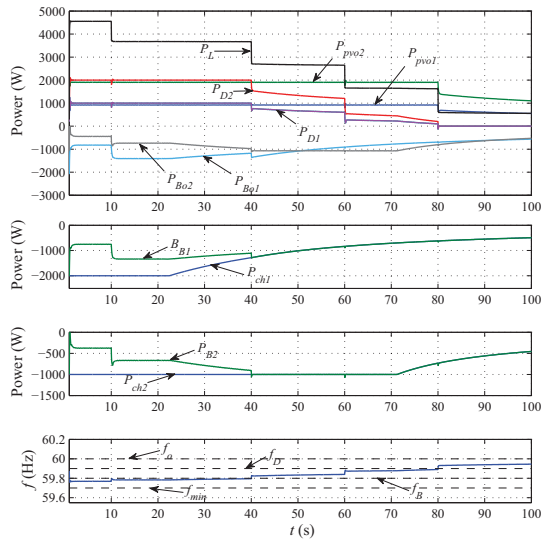
Fig. 8. Coordination of the battery units in response to *SOC* variations.

Fig. 9. Response of PV units to variations in solar irradiance during PV production curtailment.

units operate at their charging limit and cannot absorb any more energy.

C. PV Generation Curtailment

The response of the control strategy to solar irradiance variations is illustrated in Fig. 9. Initially, both PV units are curtailing their surplus PV generation to match the load demand. Between $t = 10$s and 20s, the irradiance drops from 1000 W/m^2 to 400 W/m^2. In this case, PV units decrease their PV operating voltages towards their MPPs, to keep supplying the load demand. At $t = 20$s, both units start operating at their maximum available power, and the droop units start supplying any additional load demand. Similarly, when the irradiance starts increasing at $t = 25$s, PV units increase their PV operating voltages to curtail the surplus PV generation. At $t = 60$s, the load starts increasing, hence, PV units start increasing the output power to meet the load until they reach their maximum available power again at $t = 65$s. At this point, the droop units start to pick up any further increase in the load. This scenario shows the ability of the strategy to react to irradiance changes while the PV generation is being curtailed. In this case, the control systems autonomously follow changes in the irradiance to maintain the desired level of generation required by the load. On the other hand, the behavior of the microgrid units in response to changes in the PV generation due to solar irradiance variations is shown in Fig. 10. This figure illustrates the autonomous coordination among the units to meet the load demand and to maintain the power balance in the islanded microgrid.

IV. CONCLUSION

A decentralized power management strategy is developed in this paper to coordinate PV, battery, and droop controlled units in islanded microgrids. In this strategy, the local voltage and power control loops, at each of the PV and battery units, are configured to follow multi-segment *P/f* characteristic curves. These characteristic curves can be adjusted autonomously at
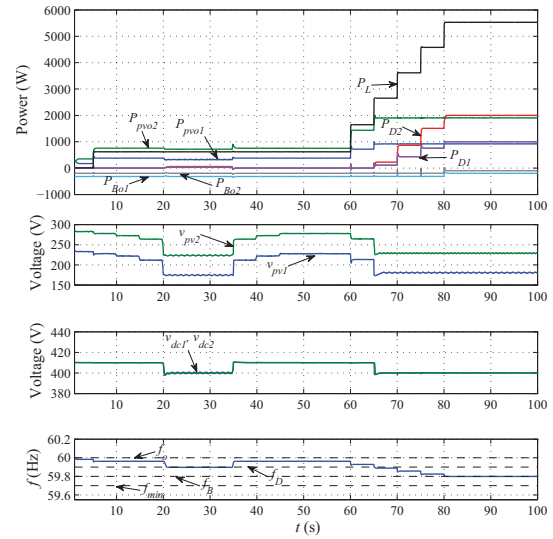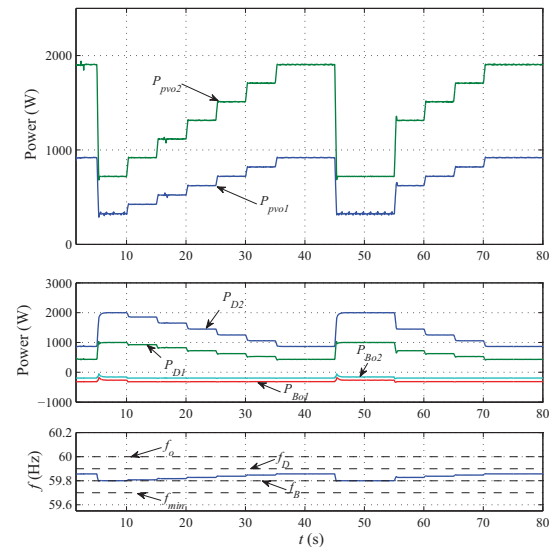

Fig. 10. Response to PV generation variations due to solar changes in solar irradiance.

each unit according to the microgrid operating conditions. It is shown that by using these adaptive *P/f* characteristic curves, a fully autonomous coordination can be achieved, without relying on any external communications and central management schemes. Also, it is shown that the multi-loop control implementation of the strategy results in smooth transitions among different control objectives. The performance of the proposed strategy has been successfully validated using a detailed switching model implemented in the PSCAD/EMTDC environment.

REFERENCES

[1] J. A. P. Lopes, C. L. Moreira, and A. G. Madureira, "Defining control strategies for microgrids islanded operation," *IEEE Trans. Power Syst.*, vol. 21, no. 2, pp. 439–449, May 2006.

[2] R. H. Lasseter, J. H. Eto, B. Schenkman, J. Stevens, H. Vollkommer, D. Klapp, E. Linton, H. Hurtado, and J. Roy, "CERTS microgrid laboratory test bed," *IEEE Trans. Power Del.*, vol. 26, no. 1, pp. 325–332, Jan. 2011.

[3] K. Brabandere, B. Bolsens, J. V. Keybus, A. Woyte, J. Driesen, and R. Belmans, "A voltage and frequency droop control method for parallel inverters," *IEEE Trans. Power Electron.*, vol. 22, no. 4, pp. 1107–1115, Jul. 2007.

[4] C. N. Rowe, T. J. Summers, R. E. Betz, D. J. Cornforth, and T. G. Moore, "Arctan power–frequency droop for improved microgrid stability," *IEEE Trans. Power Electron.*, vol. 28, no. 8, pp. 3747–3759, Aug. 2013.

[5] I. U. Nutkani, P. C. Loh, and F. Blaabjerg, "Droop scheme with considering of operating cost," *IEEE Trans. Power Electron.*, vol. 29, no. 3, pp. 1047–1052, Mar. 2014.

[6] D. De and V. Ramanarayanan, "Decentralized parallel operation of inverters sharing unbalanced and nonlinear loads," *IEEE Trans. Power Electron.*, vol. 25, no. 12, pp. 3015–3025, Dec. 2010.

[7] C. Wang and M. H. Nehrir, "Power management of a stand-alone wind/photovoltaic/fuel cell energy system," *IEEE Trans. Energy Convers.*, vol. 23, no. 3, pp. 957–967, Sep. 2008.

[8] B. Belvedere, M. Bianchi, A. Borghetti, C. A. Nucci, M. Paolone, and A. Peretto, "A microcontroller-based power management system for a standalone microgrids with hybrid power supply," *IEEE Trans. Sust. Energy*, vol. 3, no. 3, pp. 422–431, Jul. 2012.

[9] K. T. Tan, X. Y. Peng, P. L. So, Y. C. Chu, and M. Z. Q. Chen, "Centralized control for parallel operation of distributed generation inverters in microgrids," *IEEE Trans. Smart Grid*, vol. 3, no. 4, pp. 1977–1987, Dec. 2012.

[10] K. T. Tan, P. L. So, Y. C. Chu, and M. Z. Q. Chen, "Coordinated control and energy management of distributed generation inverters in microgrid," *IEEE Trans. Power Del.*, vol. 28, no. 2, pp. 704–713, Apr. 2013.

[11] J. Kim, J. Jeon, S. Kim, C. Cho, J. Park, H. Kim, and K. Nam, "Cooperative control strategy of energy storage system and microsources for stabilizing the microgrid during islanded operation," *IEEE Trans. Power Electron.*, vol. 25, no. 12, pp. 3037–3048, Dec. 2010.

[12] M. A. Abusara, J. M. Guerrero, and S. M. Sharkh, "Line interactive UPS for microgrids," *IEEE Trans. Ind. Electron.*, vol. 61, no. 3, pp. 1292–1300, Mar. 2014.

[13] A. M. Egwebe, M. Fazeli, P. Igic, and P. Holland, "Implementation and stability study of dynamic droop in islanded microgrids," *IEEE Trans. Energy Convers.*, vol. 31, no. 3, pp. 821–832, Sep. 2016.

[14] S. Sahoo and S. Mishra, "A multi-objective adaptive control framework in autonomous dc microgrid," *IEEE Trans. Smart Grid*, vol. PP, no. 99, pp. 1–1, 2017.

[15] E. Serban and H. Serban, "A control strategy for a distributed power generation microgrid application with voltage- and current controlled source converter," *IEEE Trans. Power Electron.*, vol. 25, no. 12, pp. 2981–2992, Dec. 2010.

[16] D. Wu, F. Tang, T. Dragicevic, J. C. Vasquez, and J. M. Guerrero, "Autonomous active power control for islanded ac microgrids with photovoltaic generation and energy storage system," *IEEE Trans. Energy Convers.*, vol. 29, no. 4, pp. 882–892, Dec. 2014.

[17] ——, "A control architecture to coordinate renewable energy sources and energy storage systems in islanded microgrids," *IEEE Trans. on Smart Grid*, vol. 6, no. 3, pp. 1156 – 1166, May 2015.

[18] W. Du, Q. Jiang, M. J. Erickson, and R. H. Lasseter, "Voltage-source control of PV inverter in a CERTS microgrid," *IEEE Trans. Power Del.*, vol. 29, no. 4, pp. 1726 – 1734, Aug. 2014.

[19] H. Mahmood, D. Michaelson, and J. Jiang, "Strategies for independent deployment and autonomous control of PV and battery units in islanded microgrids," *IEEE Journal of Emerging and Selected Topics in Power Electronics*, vol. 3, no. 3, pp. 742 – 755, 2015.

[20] ——, "A power management strategy for PV/battery hybrid systems in islanded microgrids," *IEEE Journal of Emerging and Selected Topics in Power Electronics*, vol. 2, no. 4, pp. 870 – 882, Dec. 2014.

[21] ——, "Decentralized power management of a PV/battery hybrid unit in a droop controlled islanded microgrid," *IEEE Trans. Power Electron.*, vol. 30, no. 12, pp. 7215 – 7229, Dec. 2015.

[22] Y. Karimi, H. Oraee, M. Golsorkhi, and J. Guerrero, "Decentralized method for load sharing and power management in a PV/battery hybrid source islanded microgrid," *IEEE Trans. Power Electron.*, vol. 32, no. 5, pp. 3525–3535, May 2017.

[23] H. Mahmood and J. Jiang, "Autonomous coordination of multiple PV/battery hybrid units in islanded microgrids," *IEEE Trans. Smart Grid*, vol. PP, no. 99, pp. 1–1, 2017.

[24] S. Adhikari and F. Li, "Coordinated V-f and P-Q control of solar photovoltaic generators with MPPT and battery storage in microgrids," *IEEE Trans. Smart Grid*, vol. 5, no. 3, pp. 1270–1281, May 2014.

[25] S. Bae and A. Kwasinski, "Dynamic modeling and operation strategy for a microgrid with wind and photovoltaic resources," *IEEE Trans. Smart Grid*, vol. 3, no. 4, pp. 1867–1876, Dec. 2014.

[26] Z. Yi, W. Dong, and A. H. Etemadi, "A unified control and power management scheme for PV-battery-based hybrid microgrids for both grid-connected and islanded modes," *IEEE Trans. Smart Grid*, vol. PP, no. 99, pp. 1–1, 2017.

[27] T. Dragičević, J. M. Guerrero, J. C. Vasquez, and D. Škrlec, "Supervisory control of an adaptive regulated DC microgrid with battery management capability," *IEEE Trans. Power Electron.*, vol. 29, no. 2, pp. 695–706, Feb. 2014.

[28] Y. Han, H. Li, P. Shen, E. Coelho, and J. Guerrero, "Review of active and reactive power sharing strategies in hierarchical controlled microgrids," *IEEE Trans. Power Electron.*, vol. 32, no. 3, pp. 2427–2451, Mar. 2016.

[29] R. H. Lasseter and P. Piagi, "Control and design of microgrid components, Final project report," Power System Engineering Research Center (PSERC), Madison, WI, Tech. Rep. 06-03, Jan. 2006.

[30] Z. Miao, L. Xu, V. R. Disfani, and L. Fam, "An SOC-based battery management system for microgrids," *IEEE Trans. Smart Grid*, vol. 5, no. 2, pp. 966–973, Mar. 2014.

[31] Y. Cao, S. Tang, C. Li, P. Zhang, Y. Tan, Z. Zhang, and J. Li, "An optimized EV charging model considering tou price and soc curve," *IEEE Trans. Smart Grid*, vol. 3, no. 1, pp. 388–393, Mar. 2012.

[32] P. Thounthong, S. Rael, and B. Davat, "Control algorithm of fuel cell and batteries for distributed generation system," *IEEE Trans. Energy Convers.*, vol. 23, no. 1, pp. 148–155, Mar. 2008.

[33] R. F. Nelson, "Power requirements for batteries in hybrid electric vehicles," *J. Power Sources*, vol. 91, no. 1, pp. 2–26, Aug. 2000.

Hisham Mahmood (S'10-M'15) received the Ph.D. degree in Electrical Engineering from The University of Western Ontario, Canada, in 2014, and the M.E.Sc. degree in Control Engineering from Lakehead University, Canada, in 2008. He is currently a Research Fellow with the Department of Renewable Energy, University of Exeter, Cornwall, UK.

He was a Postdoctoral Associate with the Department of Electrical and Computer Engineering, The University of Western Ontario, Canada, during 2015-2017. His research interests include modeling and control of switching power converters, distributed generation, renewable energy integration, microgrids, power quality, and power generation planning and control.

Jin Jiang (S'85-M'87-SM'94-F'17) received the Ph.D. degree from the University of New Brunswick, Fredericton, NB, Canada, in 1989. Since 1991, he has been with the Department of Electrical and Computer Engineering, The University of Western Ontario, London, ON, Canada, where he is currently a Senior Industrial Research Chair Professor. His research interests include fault-tolerant control of safety-critical systems, advanced control of electrical power plants, and power systems involving renewable energy resources.

Dr. Jiang is a Fellow of Canadian Academy of Engineering. He is also a Member of the International Electrotechnical Commission (IEC) 45A subcommittee to develop industrial standards on instrumentation and control for nuclear facilities. He also works closely with the International Atomic Energy Agency (IAEA) on modern control and instrumentation for nuclear power plants.